

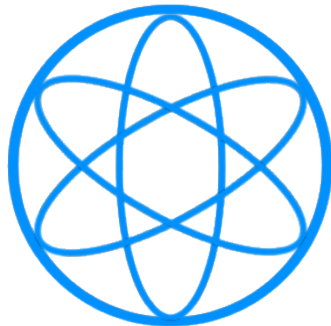
TECHNISCHE UNIVERSITÄT MÜNCHEN



ABSCHLUSSARBEIT IM MASTERSTUDIENGANG
KERN-/TEILCHEN-/ASTROPHYSIK

Programming and Installation of a New 11-inch Telescope Subsystem for MAGIC

*Programmierung und Installation eines neuen 11-Zoll-Teleskopsystems für
MAGIC*



Physik Department TUM



Max-Planck-Institut für Physik

Daniel Hoff

Erstgutachter (Themensteller): PD Dr. Oliver KORTNER
Zweitgutachter: Prof. Dr. Lothar OBERAUER

March 24, 2020

Abstract

This thesis is about the installation of a new subsystem for the MAGIC telescopes on La Palma with the purpose of measuring the atmospheric transmission simultaneously to the regular data taking in order to improve the ability to correct for atmospheric fluctuations at very high zenith angle observations.

The thesis includes the physical build-up as well as the programming of it.

Zusammenfassung

Diese Masterarbeit beinhaltet die Installation eines neuen Subsystems für die MAGIC-Teleskope auf La Palma. Ziel ist es, die atmosphärische Transmission zeitgleich zur regulären Datennahme zu messen, um diese speziell bei Messungen in hohen Zenitwinkeln besser um die von atmosphärischen Fluktuationen verursachten Schwankungen zu korrigieren.

Die Arbeit beinhaltet sowohl den physischen Aufbau des Subsystems als auch dessen Programmierung.

Acknowledgement

At this point, I want to give special thanks to Jürgen Besenrieder for his daily support during my work on this thesis including the technical support on physically building up the telescope on La Palma as well as the general availability and help with every day problems. Furthermore, I want to thank the MAGIC team for giving me regular input and advises.

Contents

Abbreviations	2
1 Introduction	3
1.1 The subject of this thesis	3
1.2 Physical background	3
2 The influence of the atmosphere on the propagation of Cherenkov light	11
3 MAGIC Atmosphere Minion	15
3.1 Assembly	16
3.2 Main task	19
3.2.1 Communication with the central control	19
3.2.2 Regular measurements	20
3.2.3 Star guiding	20
3.2.4 Advanced controls	21
3.2.5 Data calibration	24
3.2.6 Additional telescope tube and secondary camera	25
4 Measurement test run	26
4.1 Measured object	26
4.2 Comparison with the atmospheric model	30
4.3 Comparison with photometry of the secondary camera	30
4.4 Comparison with the LIDAR results	32
5 Conclusion and outlook	33
A Data	34
B Source code	36
C References	37

Abbreviations

MAGIC-Telescopes	Major Atmospheric Gamma-Ray Imaging Cherenkov Telescopes
MAM	MAGIC Atmosphere Minion
LST	Large Sized Telescopes
CTA	Cherenkov Telescope Array
IACT	Imaging Atmospheric Cherenkov Telescope
VHE	Very High Energy
AGN	Active Galactic Nuclei
SMBH	Super Massive Black Hole
SNR	SuperNova Remnant
VLZA	Very Large Zenith Angle
CR	Cosmic rays
MIDAS	Munich Image Data Analysis System
LIDAR	LIght Detection And Ranging system

1 Introduction

1.1 The subject of this thesis

For ground based very high energy γ -ray astronomy imaging air-shower Cherenkov telescopes (IACT) are used. These are telescopes that observe the secondary radiation of cosmic particles, which hit the atmosphere. This means that the atmosphere itself is used as a calorimeter for the cosmic rays. It is important to know the transmission changes in atmosphere, since they are influencing the detectable light.

The subject of this thesis was to install a new additional optical telescope (MAM) for MAGIC, which improves the determination of the transmission changes in the atmosphere. Specifically it will enable a wavelength dependent correction of the atmospheric transmission in real time to be able to correct the MAGIC data for atmospheric fluctuations. This is especially necessary for very large zenith angle observations (VLZA), i.e. observations close to the horizon.

The subject includes writing a control software for this new subsystem to ensure fully automatic operation.

In this thesis there first will be an overview over the astrophysical background, followed by a description of atmospheric effects. After that the MAM telescope will be introduced by the description of the hardware followed by the description of its task and the principle software implementation of it. Next, there will be an exemplary analysis of a test measurement to show the working principle and the functionality. In the end, there will be an outlook to the further use of the telescope.

The data of the test run can then be found in the appendix.

1.2 Physical background

Goals of astroparticle physics

Astroparticle physics is an area of physics that uses cosmic rays as messengers for obtaining information about the processes going on in space. Cosmic rays are all kinds of particles flying unbound through the universe. Examples are protons, electrons, anti-protons, atom cores, neutrinos or photons. In fundamental research like astroparticle physics, one tries to push forward the boundaries of understanding the universe. Therefore the observation of different types, sources and energies of messengers is important. While it is easier to measure particles in low energy ranges, there are problems at higher energies. First, there are not so many particles at higher energies (e.g. above one TeV, there are no sources with a flux above 10^{-7} particles per second and square meter)[2]. Second, the higher the energy, the less probable it is for the particle to interact with the detector. Therefore the maximum energy a common detector can measure is limited. At the moment Fermi (launched 2008) is the satellite that measures the highest energies (up to 300 GeV).

For particles with higher energies it is best to use Imaging Air-shower Cherenkov Telescopes. Currently there are three experiments using this technique: MAGIC (30 GeV to 100 TeV, start 2004[1]), HESS (30 GeV to 100 TeV, start 2002[3]) and VERITAS (50 GeV to 50 TeV, start 2005[4]).

Sources and messengers

To obtain further understanding of ongoing processes in the universe, it is important to determine the origin of the measured particles. Charged particles are always bouncing off

magnetic fields, which are omnipresent in space. Therefore their primary origin can't be determined, but the origin of acceleration (see Fig. 1). For neutral particles like neutrinos and photons for example, the origin can be reconstructed by interpolation.

Figure 1 shows the occurrence of different particles in different energy regions as well as their origin.

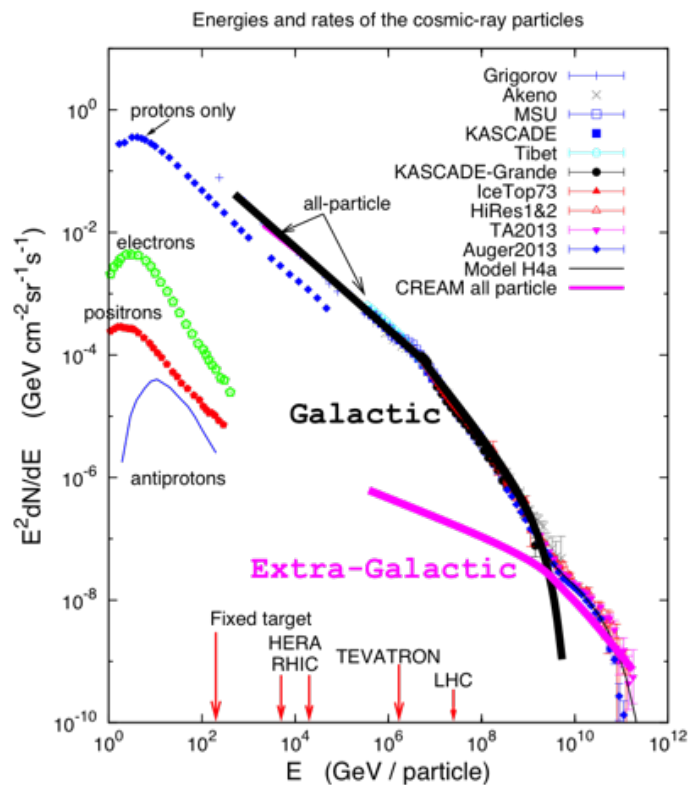


Figure 1. Energies and rates of cosmic rays with sources. Source: [5]

Sources that are observed by the MAGIC telescopes are depicted in Figure 2. In the galaxies there are for example supernova remnants (SNRs), which are the outer gaseous shells of stars that recently exploded in a supernova. They are thought to produce and accelerate cosmic rays via diffusive shock waves which will therefore produce highly energetic charged particles. Due to inverse Compton scattering or bremsstrahlung for example this will emit gamma rays as well. Therefore spectra of young SNRs are needed. One of the SNRs MAGIC is regularly observing is the Crab nebula in the Taurus constellation.[1] (See fig. 3)

The maximum energy a particle can be accelerated through a SNR shock front is in the order of 10^7 GeV. This is the origin of the knee feature (the bend in Figure 1 at 10^7 GeV).

Another source type are active galactic nuclei (AGN), which contain a super massive black hole (SMBH). While these are absorbing mass, they produce particle jets at their rotation axes. An example for this is the centre of the milky way. The number of known AGNs increased drastically in the last 10 years due to IACTs.[1]

Furthermore pulsars and pulsar wind nebulae are sources for VHE photons. Pulsars are highly magnetic, fast rotating neutron stars, accelerating CRs up to a few GeV. An example for such a pulsar is the Crab nebula, a SNR.[1]

Another source of interest are gamma ray bursts, which are very bright gamma events that occur about once per day and last normally some seconds to some minutes.[1]

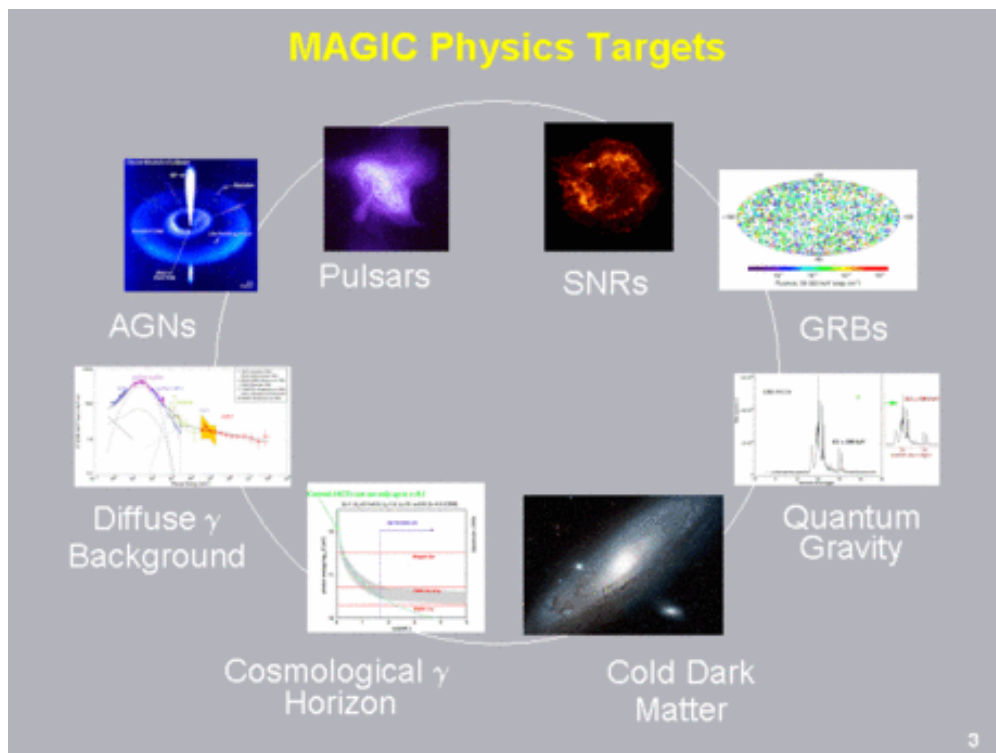


Figure 2. Sources of interest observed by MAGIC. Source: [1]

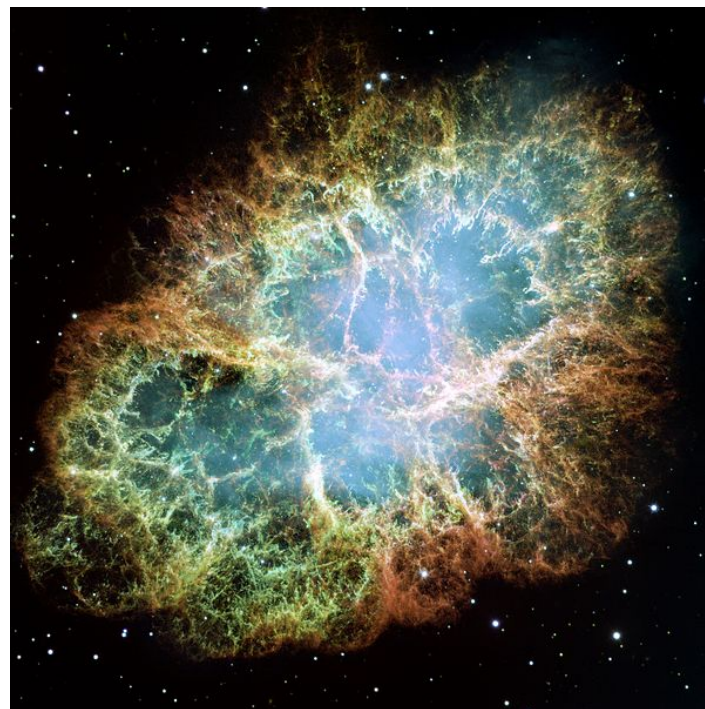


Figure 3. The Crab nebula. Source: [6]

Air showers and Cherenkov radiation

When VHE cosmic rays hit the atmosphere, they start a cascade of particles. This happens due to inelastic scattering at the particles of the air, which produces new particles. Every secondary particle will further expand the shower until the shower particles energies are too low to create new particles or until the particles reach the ground. The shape of the shower depends mostly on the type of primary particle that hits the atmosphere. Figure 5 shows that the heavier the incoming particle, the more diffuse and broad the shower becomes. This happens, because photons and electrons produce showers that mostly consist of e^+/e^- pairs and γ -radiation, while heavier CRs create a significant amount of hadrons (e.g. pions) with a higher transverse momentum. (see Fig. 4)

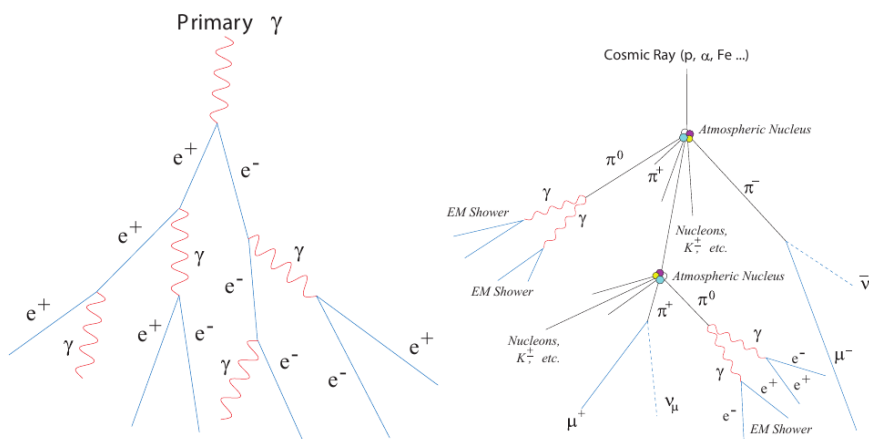


Figure 4. Composition of a shower induced by a gamma (left) and a proton (right). Source: [7]

If a charged particle travels faster than light in a medium i.e. $v_{particle} > c/n$ it creates an electromagnetic shock front (see Fig.6), because the particle travels faster than the induced polarisation of the medium. This shock front is visible as blue light. The colour is blue because the higher energetic light (uv) is stronger absorbed by air. The angle of this front cone is given by Equ. 1. The frequency spectrum can be calculated with Equ. 2.[9]

$$\cos(\theta) = \frac{c}{vn(\omega)} \quad (1)$$

$$\frac{d^2E}{dx d\omega} = \frac{q^2}{4\pi} \mu(\omega) \omega \left(1 - \frac{c^2}{v^2 n^2(\omega)} \right) \quad (2)$$

Equations 1, 2. θ is the angle of the radiation cone, ω is the angular frequency, μ is the frequency dependent magnetic permeability, $d^2E/dxd\omega$ is the amount of energy emitted over a distance x per frequency, q is the electric charge, c is the speed of light in vacuum, v the velocity of the particle and n is the frequency dependent refractive index.

With the energy of the Cherenkov light the energy of the primary gamma ray can also be reconstructed. Since the Cherenkov light is typically emitted in a circle with 250 m diameter, it produces only a few photons per square meter. Therefore the sensitivity of the instruments must be as high as possible. Also big light collecting areas are needed. (The MAGIC telescopes have 17m diameter for example) To reduce background light, these telescopes are often build

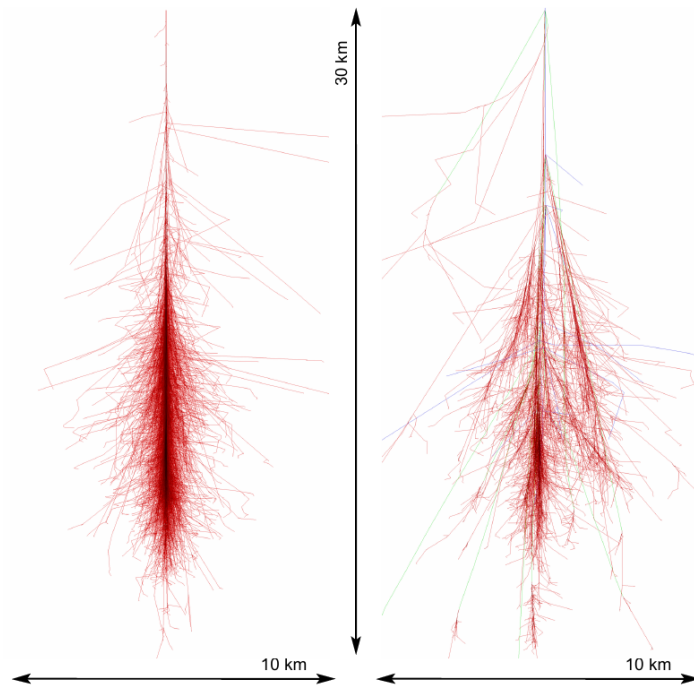


Figure 5. Shower of a gamma (left) and a proton (right). Source: [7]

upon mountains with very low light pollution. This also decreases the risk of clouds preventing measurements.

As described above, charged particles produce a wider spread out shower of secondary particles. Hence they cause a quiet uniform background in contrast to VHE gamma events. Therefore and due to their difference in shape of the showers fairly clean gamma events can be separated out of the data even though gamma events are much rarer than proton events. Furthermore, there are muon events to be separated from the gamma events. This is rather simple, since muons are mostly interacting with the atmosphere very close to the ground, so they form visible rings in the images.

An example of a muon induced event and a γ -induced event are shown in Figure 7.

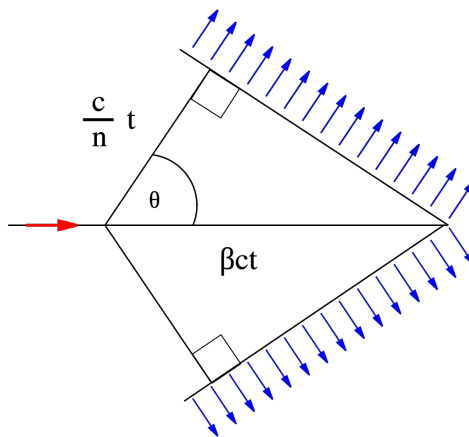


Figure 6. Cherenkov effect (ideal case without dispersion). Source: [9]

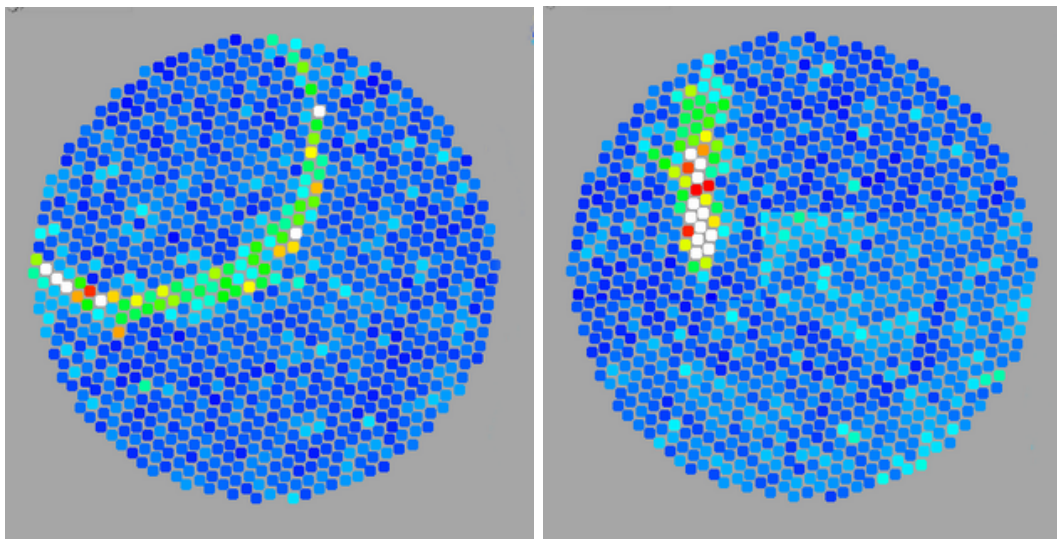


Figure 7. Event induced by a myon (left) and a gamma ray (right).

The MAGIC telescopes

The MAGIC telescopes are two IACTs with a diameter of 17 m each and a distance of 85 m from each other. They are installed on the Roque de los Muchachos on the canary island La Palma at a height of 2225 m above sea level.

To obtain an image of an object measured by IACTs a reconstruction based on the Hillas-parameter analysis is needed. As seen in figure 7 on the right, a gamma event has an elliptical shape. From this ellipse the Hillas-parameter can be determined as illustrated in Figure 9. With these, the shower energy and direction can be determined. The shower direction is reconstructed by calculating the intersection point of the shower's main axes from all telescopes. [10]

In Figure 10 one can see the Crab nebula as it is measured with the MAGIC telescopes. One clearly sees the gamma ray source (energy above 100 GeV) which is caused by shock wave acceleration in the nebula. Obviously, the resolution can't compete with optical images like from Hubble space telescope (see Fig. 3) but that is not necessary. Instead the sensitivity to detect single photons is required. The existence and the intensity of VHE gamma rays is

1. INTRODUCTION

enough to gain the information needed to produce models to describe the object.[1]



Figure 8. MAGIC site image

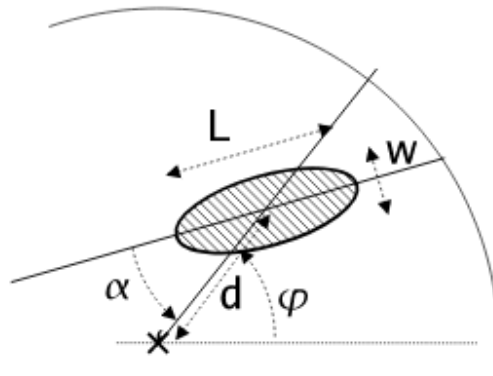


Figure 9. Geometrical definition of the Hillas parametrs. Source: [10]

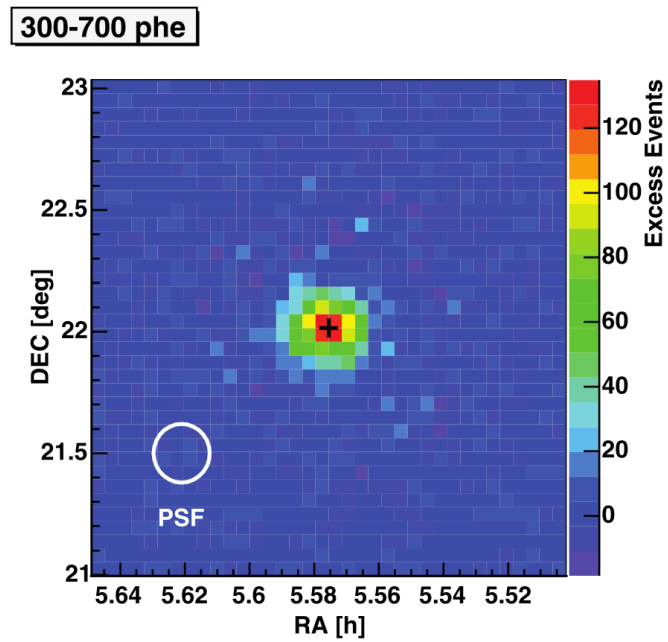


Figure 10. The Crab nebula seen through MAGIC. Source: [1]

2 The influence of the atmosphere on the propagation of Cherenkov light

Scattering processes

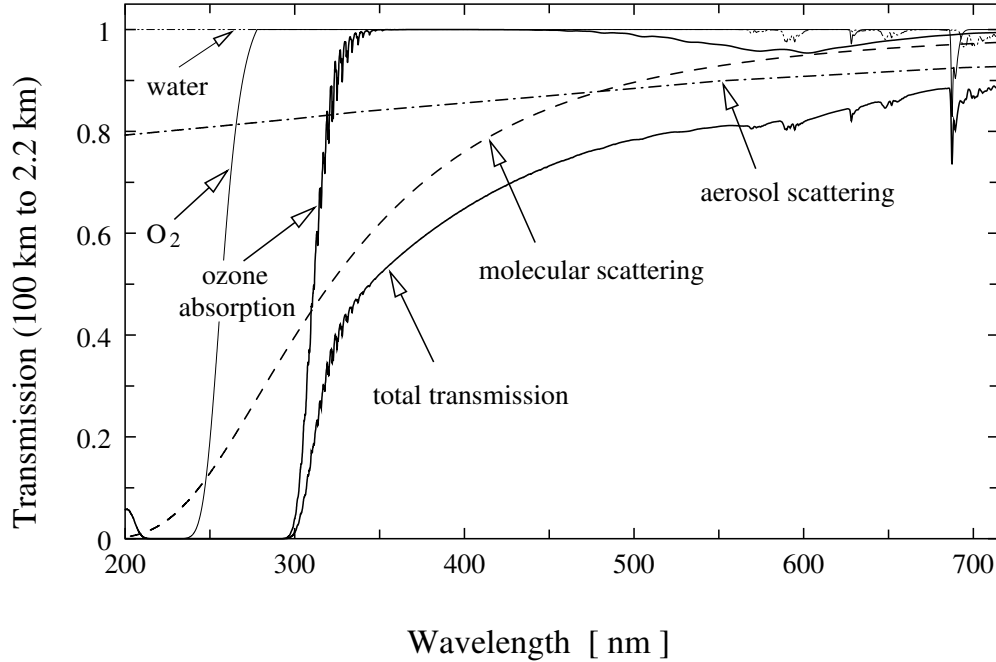


Figure 11. The effects of different absorption and scattering mechanisms and their wavelength dependence on light from space. Source: [11]

When light passes through the atmosphere, there are different mechanisms that influence its passage. First, air consists of atoms by which light can be scattered (Rayleigh-scattering). Second, there are aerosols by which light can be scattered (Mie-scattering) or absorbed. Figure 11 shows the wavelength dependence of the Mie-scattering (aerosols), of the Rayleigh scattering (molecular) and of the absorption of water, oxygen and ozone, as well as the resulting total transmission.

Mie scattering can be the scattering at any aerosol particles in the air like water vapour, sand (e.g. Calima, see Fig. 12), smoke.

Rayleigh scattering describes the elastic scattering of an electromagnetic wave by particles much smaller than the wavelength of the radiation. For light frequencies much smaller than the resonance frequency of the scattering particle, the cross section of the scattering is given by Equation 3 [13]

$$\sigma = \frac{8\pi d^6 k^4}{3} \left(\frac{\left(\frac{n_2}{n_1}\right)^2 - 1}{\left(\frac{n_2}{n_1}\right)^2 + 1} \right)^2 \quad (3)$$

Equation 3. Cross section of Rayleigh scattering with the wave number $k = 2\pi/\lambda$, the diameter of the particle d and n_1 and n_2 the refractive index of the air and the particle. The intensity given by Equation 4:

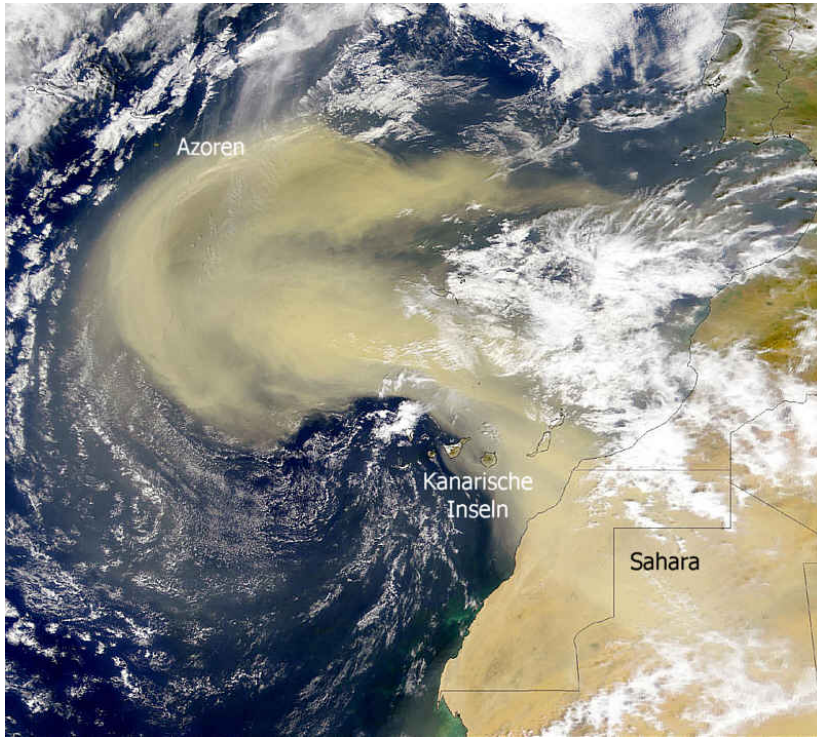


Figure 12. Calima. Weather condition with east wind on the Canary islands bringing sand from Sahara into the air. Source: [12]

$$I = I_0 \left(\frac{1 + \cos^2 \theta}{2R^2} \right) \left(\frac{2\pi}{\lambda} \right)^4 \left(\frac{n^2 - 1}{n^2 + 2} \right)^2 \left(\frac{d}{2} \right)^6 \quad (4)$$

Equation 4. Light intensity of Rayleigh scattering: d is the diameter of the particle, θ is the scattering angle, n is the refractive index of the particle, I_0 is the light intensity before the interaction and R is the distance between particle and observer. [14]

Physically, the Rayleigh scattering is caused by the electric polarisation of a particle. The oscillating electric field of light induces a fluctuating dipole in the particle. Thus the particle starts radiating. This can happen as well at atoms or small molecules.

In air, this causes the diffuse sky lighting, since the sunlight is scattered in the atmosphere. From Equation 3 one can see that blue light is scattered much stronger than red light (see Equ. 5). Since the human eye is not as sensitive to violet light as to blue, this causes the sky background to be blue during day and red during sunset. [13]

$$\frac{\sigma_{blue}}{\sigma_{red}} = \frac{\frac{1}{\lambda_{blue}^4}}{\frac{1}{\lambda_{red}^4}} \approx \left(\frac{650 \text{ nm}}{450 \text{ nm}} \right)^4 \approx 4.4 \quad (5)$$

Mie-scattering or Mie-Lorenz-scattering on the other hand describes the scattering of a electromagnetic wave off a homogeneous sphere. It takes only place in the troposphere (mainly in the lower 4.5 km). Mathematically it is an infinite series of spherical multipole partial waves as a solution to Maxwell's equations. [14] The different angular distributions of scattered light depending on the type of scattering can be seen in Figure 13.

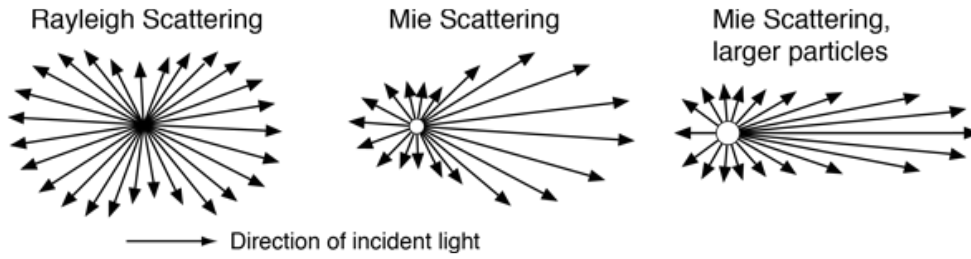


Figure 13. Angular dependence of light scattering by particles smaller than (left), similar to (middle) and larger than the wavelength of the light. Source: [15]

Very large zenith angle observation

When light travels through a medium, its intensity decreases exponentially. The extinction is described by the Beer–Lambert law (equ. 6):

$$E_\lambda = \log_{10} \left(\frac{I_0}{I_1} \right) = \varepsilon_\lambda \cdot c \cdot d \quad (6)$$

With the extinction E_λ , the intensity of the incoming light I_0 , the intensity of the outgoing light I_1 , the molar concentration c , the extinction coefficient ε_λ and the distance d the light travels through the medium.[19]

To correct data from a telescope, a standard model for the atmosphere can be used. This uses the air mass (amount of air in the line of sight till space, while zenith has an air mass of one) and the average scattering expectation value. This works fine, if not too many aerosols and disturbances are in the atmosphere. However, if the telescopes are pointing closer to the horizon, the air mass increases with about $\sim 1/\cos(\phi)$ the zenith angle ϕ (see Equ. 7, Fig. 14, 15). Therefore the risk of deviation from the ideal model increases as well.

$$X = \sqrt{\left(\frac{R_E + y_{\text{obs}}}{y_{\text{atm}}} \right)^2 \cos^2 z + \frac{2R_E}{y_{\text{atm}}^2} (y_{\text{atm}} - y_{\text{obs}}) - \left(\frac{y_{\text{obs}}}{y_{\text{atm}}} \right)^2 + 1} - \frac{R_E + y_{\text{obs}}}{y_{\text{atm}}} \cos z \quad (7)$$

Equation 7. Air mass X with radius of earth R_E , elevation of observer above sea level y_{obs} , height of atmosphere above observer y_{atm} and zenith angle of observed object z .

The resulting air mass is plotted in Figure 15.

On the other hand, more air mass leads to more "detector volume". Since higher energetic gamma rays have a lower rate of getting detected, they are therefore better detectable at VLZA.

To correct for the higher amount of scattering and absorption at VLZA, there is a LIDAR (LIght Detection And Ranging system) installed at the MAGIC telescopes. This sends a green laser beam into the sky and uses the amount of reflected light to calculate the atmospheric absorption in the current observation area. However, as seen in Figure 11, this absorption can differ drastically for different wavelengths. Furthermore, the LIDAR has a maximum range of 12 km. Therefore, additional information on the atmospheric conditions are needed for VLZA observations.

The subject of this thesis was to install a new subsystem (MAM) that measures the atmospheric transmission in dependence of the wavelength. It measures the light passing through the

2. THE INFLUENCE OF THE ATMOSPHERE ON THE PROPAGATION OF CHERENKOV LIGHT

whole atmosphere and is therefore not restricted in range, unlike LIDAR. The data obtained by MAM is then used to correct the data of MAGIC.

This thesis includes the assembly as well as the programming of this new subsystem. It is described in detail in the following section.

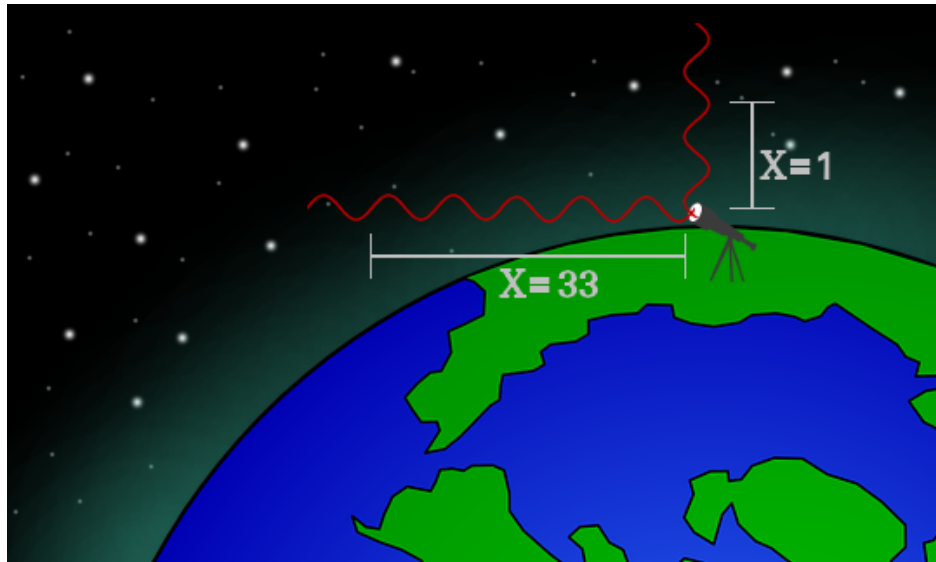


Figure 14. Increasing of the air mass with the zenith angle.

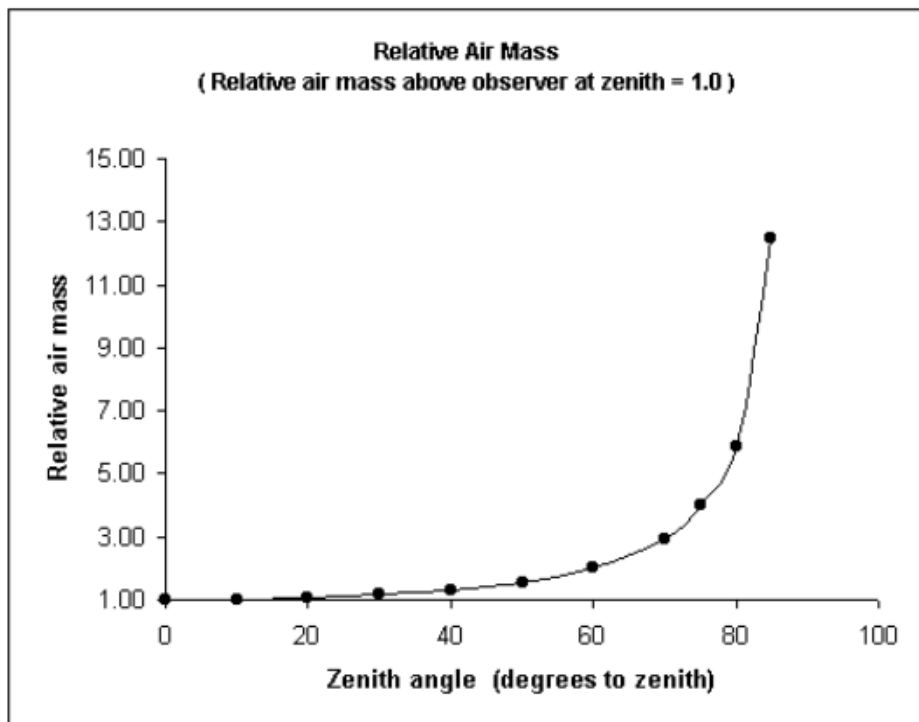


Figure 15. Increasing of the air mass with the zenith angle according to Equ. 7.

3 MAGIC Atmosphere Minion



The dome, the control PC and the MAM telescope.

The MAGIC Atmosphere Minion (MAM) is a subsystem to the MAGIC telescopes. It is meant to measure the atmospheric conditions in the direct neighbourhood to the observation target of the MAGIC telescopes simultaneously to the data taking of MAGIC. MAM therefore measures the wavelength dependent intensity of a nearby star and compares this to the expected intensity to obtain the atmospheric transmission.



The MAGIC-1 Telescope together with the MAM telescope.

3.1 Assembly

The MAM telescope consists of two telescope tubes, three cameras, one filter wheel, one spectrograph and a mount.

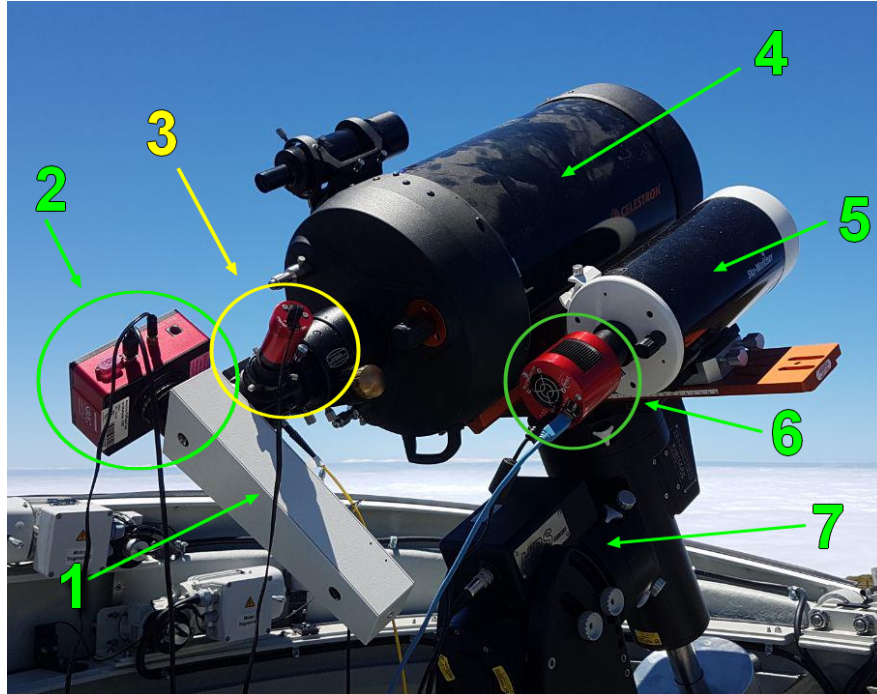


Figure 16. Assembly of the MAM Telescope:

1: Spectrograph 2: Main camera 3: Slit camera 4: Main telescope 5: Small guiding telescope 6: Guiding camera 7: Mount.

The main tube is a Celestron C11 telescope tube. It has an eleven inch main mirror and is a Schmidt-Cassegrain with a focal length of 2800 mm.

The spectrograph is a Baches Echelle Spektrograf with two slits of $25 \mu\text{m}$ and $50 \mu\text{m}$ width. Its spectral range goes from 392 nm to 800 nm with a wavelength resolution of $R = \lambda/\Delta\lambda = 10^4$. It is directly mounted onto the main telescope tube.

To control that a star hits the slit correctly, there is a small slit camera of type ZWO ASI Mini mounted onto the spectrograph. An example image of a star hitting the slit is shown in Figure 17.

The main camera is a SBIG STF-8300. It observes the spectral lines after the light of the observed star is split in the spectrograph. It is a 16 bit camera with a size of 3352×2532 pixel and a typical readout noise of $10 e^-$ (RMS). It has a cooler with fan and is by default set to a CCD temperature of -20°C .

There is a small five inch Skywatcher telescope tube with a ZWO ASI Cool CMOS camera and a filter wheel next to the main tube. It was originally planned to be used as a guiding camera but has become obsolete in this respect. Therefore it now is available to be used for example for photometry. It has a CMOS sensor with a size of 4656×3520 . With the Skywatcher telescope, the field of view is 39.1×29.6 arcmin.

Finally there is the "10Micron GM 2000 HPS II Ultraport" mount. It has absolute encoders with a positioning and tracking accuracy of $<20''$ and $1''/15\text{min}$.

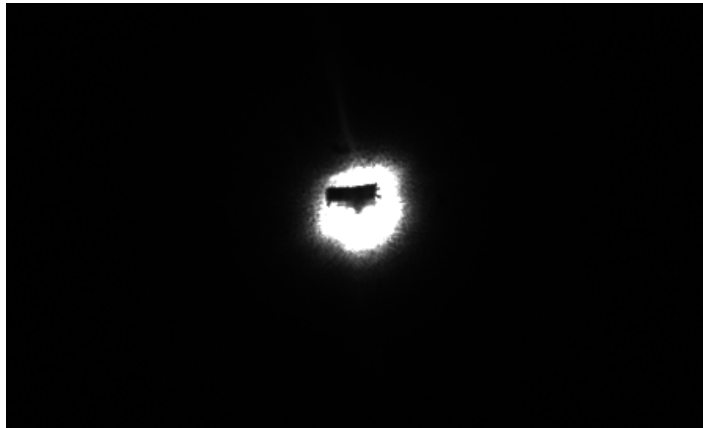


Figure 17. The star Kochab on the slit taken by the slit camera.

Baches Echelle Spektrograf

The Baches Echelle Spektrograf is a professional spectrograph build by Baader Planetarium. It splits the light two times to allow the light to be distributed in two dimensions. This allows to use the full area of a normal CCD camera chip, while having the complete spectrum visible at once. A spectrum of the star Arcturus taken through the main camera is seen in Figure 18.



Figure 18. Spectrum of Arcturus split up by the Baches Echelle Spektrograf.

As seen in Figure 19 incoming light first hits a grating plate which reflects the light and splits it up. This is called a Echelle grid. The incident angle on the grid is close to perpendicular to make use of the light of high spectral orders (between 30 and 56). This allows for a more homogeneous light in all wavelengths.

After the light is split up the first time, the different orders of the spectral lines are partially overlapping. At this point the light passes through another grid that splits the light again but

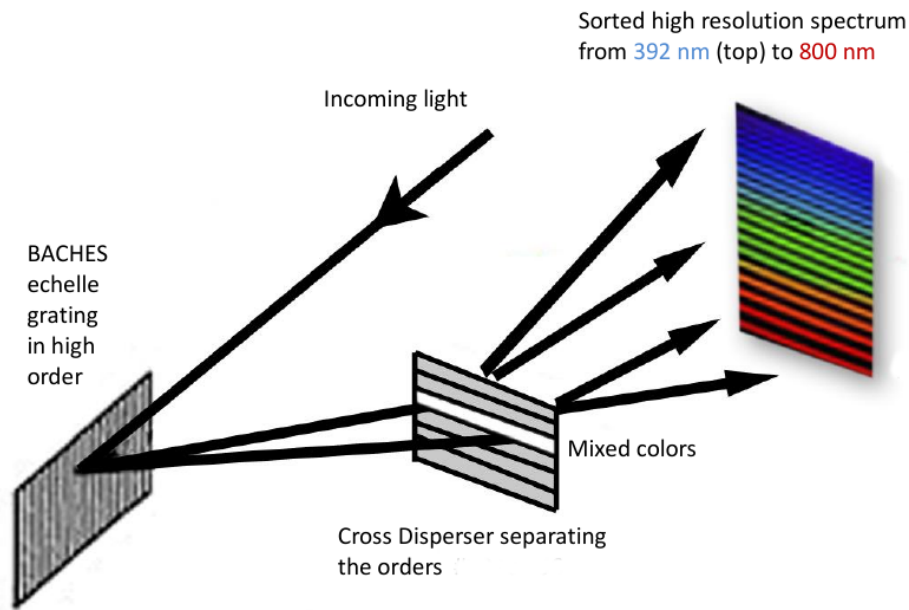


Figure 19. Schematic path of light in the spectrograph.[16]

in orthogonal direction, the spectral lines are distributed on a two dimensional surface. Due to the partial overlap before, the end of a horizontal line is repeated at the beginning of the next line.

Charge coupled device cameras

CCD sensors are light sensitive electrical circuits that use the photo effect and are often used for cameras. They were first invented as memory chips, but soon their light sensitivity was discovered. For its invention, Willard Boyle and George E. Smith got the physics nobel price in 2009.[17]

CCD can get a quantum efficiency (ratio of incoming photons to detected electrons) of nearly 100%. Therefore, they tend to be better than CMOS sensors (Complementary metal-oxide-semiconductor), but they are more expensive. Still, CMOS have partially caught up since they're widely used in mobile cameras and therefore have had a development boom in the recent years.

CCDs are composed of arrays of photo sensitive silicon semiconductor photo diodes. It is structured in electric corrals in which an electron is hold, when it was moved into the conduction band by a absorbed photon. This results in an accumulation of electrons in the corrals. At the end of the exposure, repeatedly the top row is serially read out and then the rows are shifted one row to the top. On read-out, the number of electrons is multiplied by the gain (also known as ADU = Analog-to-Digital-Unit), which often is set to:

$$G = \text{full well capacity of a pixel} / \text{pixel data size (e.g. } 2^{16} \text{ for a 16 bit image)}$$

Noise:

There are different types of noise that can occur: The read noise is the fluctuation in read-out and therefore independent of the exposure time. Since this is randomly around the actual pixel value, it could become negative, but the data format would not allow this. Therefore a bias is added to the image. After subtracting the bias value/bias image, one has the actual

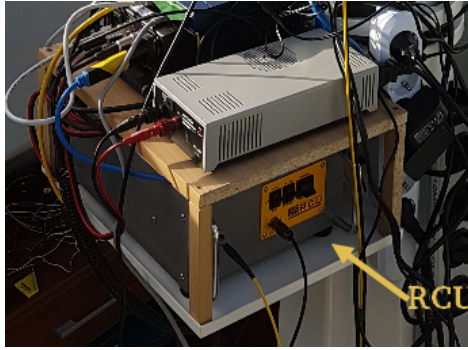


Figure 20. Remote Calibration Unit

positive and negative values of the image and can correctly handle the noise. The dark current noise is the thermal noise inside the camera chip. The noise depends on the exposure time t_{exp} . It's absolute amount is increasing with $\sqrt{t_{exp}}$ while the signal increases with t_{exp} . Therefore the signal to noise ratio increases with $\sqrt{t_{exp}}$. The dark current noise can also be reduced by cooling the CCD chip.

For the STF-8300, I measured a average dark noise of $88/2^{16}$ and $56/2^{16}$ at -10 and -20°C in a dark image of 180 s exposure time. As the bias does not differ too much from the darks, a "master-dark" image will be used for all images. It is generated by averaging over 10 darks with a exposure time of 180 s.

Remote calibration unit (RCU)

The remote calibration unit is a device that is needed for calibration of MIDAS (see Sec. 3.2.5). It has a halogen lamp for producing flat field images, as well as a thorium argon lamp for an order reference image to calibrate the spectra. MIDAS uses this image combined with a table of the known spectral lines of a ThAr lamp for calibration. Due to this, MIDAS can determine the exact wavelength of a spectrum from an image later given to it for analysis. The RCU also controls the mirror to switch between the lamps or the telescope illuminating the spectrograph.

The computer

The computer is an Intel Power-Edge with Linux Mint 19.1. It controls remote power switches for the cameras, the mount and the RCU.

3.2 Main task

3.2.1 Communication with the central control

The communication to the central control (CC) works via TCP/IP.

MAM sends its status every second to the CC. The Status information of the CC, which contains the weather warnings as well as the target of the MAGIC telescopes is send every 10 seconds to MAM.

If the control software runs in automatic mode, the check function "weather()" is called every ten seconds. This function will start the measurement if the status report received by the CC contains a valid target. If instead "PARK" is the current target or the weather information contains a warning, the measurement will be quit.

The status report send from MAM to the CC looks like the following:

```
"MAM-REPORT M0 stat cur_time com_stat rec_time dome_stat OVER\n"
```

The parameters are as follows:

stat: Status of the Telescope:

[1: Error, 2:Error in 2nd cam but else working, 3: idle, 4: working]

cur_time: The current UTC time.

com_stat: Status of the communication with the CC:

[1: Received report, 2: Connection to CC lost]

rec_time: Time at which I received the last CC-report.

dome_stat: Status of the dome [0: disconnected, 1: closed, 2:open]

3.2.2 Regular measurements

The MAM control software is started and the devices are powered on by cron (Unix program to schedule scripts) every day at 4pm UTC. Then the telescope remains idle until a target position is received by the CC-report. If so, the software looks for a bright ($\text{mag} < 6$) and non variable star close to the target of MAGIC and slews to it. The main camera obtains a spectrum of the reference star (e.g. Fig[18]) aiming for about $1/3$ saturation. After bias subtraction the image is scaled to an equivalent of 180s exposure. This image is then automatically passed to MIDAS to obtain the wavelength distribution of the star light which is stored in a fits-file. This can be used for the data correction later.

Simultaneously to the taking of the star spectrum, the secondary camera is taking images with use of the filter wheel. (r, g, b, l) These images are used for photometry in the later correction.

The telescope goes to park position, as soon as no target is given by the CC-report anymore, but latest at 9 UTC. At 9:15 UTC the devices are powered off, since after that no measurements take place.

3.2.3 Star guiding

To measure the spectrum of a star, the telescope has to be positioned such that the star is lighting onto the slit. Therefore, after the telescope has moved to a star of interest, the star should be visible in the field of view of the slit camera. If this is the case, it will correct the position of the star to the position of the slit. The position of the slit is redetermined by the software automatically after the slewing to the target. The transformation of pixel to Ra/Dec coordinates is calculated from data obtained by a reference movement. At the moment this reference movement is done every time new. In the future, it will be calculated from a existing reference movement information.

In the case, the star is not in the field of view or there are more than one very bright stars in the field of view, Astrometry is used to set the star precisely to the slit. The further correction works like before, but the "bright spot" used as the star is only searched for in the near region around the slit position.

Astrometry is a software that determines the celestial coordinates of an image of stars. It compares the angles and relative brightness of the stars in a image of stars given to it and compares it to star catalogue data. Therefore it can determine the position in the sky, the image was taken from. See also Astrometry website: <http://astrometry.net/>.

In theory, the width of the star in the plane of the slit would be given by the Airy disk (Equ. 8):[18]

$$r = f \cdot 1.22 \cdot \lambda/D = 2.800 m \cdot 1.22 \cdot \lambda/0.280 m \quad (8)$$

With the focal length f , the optics diameter D and the wavelength λ .

For red (750 nm) and blue (400 nm) light, this gives $9.15 \mu\text{m}$ and $4.88 \mu\text{m}$. Since the slit is $50 \mu\text{m}$ broad, the star should be completely inside the slit. The reason, why it is not, is, that the star is moving on the image due to seeing (atmospheric turbulences due to temperature gradients) and vibrations of the telescope (e.g. through wind). Therefore, the star light will never be completely on the slit and never completely captured by the main camera. If the amount of light missing the slit would be constant, this would not matter. But since the turbulences are random, there is need for correction.

3.2.4 Advanced controls

Apart from the default operation mode, the control software can be started by hand. The command "mam -auto" is used by cron. In the case that one wants a spectrum of another star or in general has a different task for the telescope, the interpreter can be accessed by the command "mam -manual". This could be interesting especially during full-moon break, since MAGIC isn't operating then. The exact commands are displayed upon start of the software. Additional parameters can be listed with "mam -help". In manual mode, the telescope can be used completely unrestricted, it won't react to the CC report unless it is explicitly told to.

Software commands

Since the software is the essential part of this thesis, I'll shortly introduce most of the commands that can be executed. A picture of the interpreter is shown in Figure 21.

```

Note that you can do nearby any free python input.
If you do a free input command, you are asked to confirm that the command is written correctly.

In [0]: start Tel Dom

new device 10micron

Log @2020-02-24T15:31:50
Telescope is now tracking sidereal.

new device Baader Dome

In [1]: goto Vega -h

Log @2020-02-24T15:32:04
Found: [b*' alf Lyr', '18 36 56.3363', '+38 47 01.280']

Log @2020-02-24T15:32:04
Moving to 18.626285, 38.800810

In [2]: 

```

Figure 21. Screen shot of the interpreter running in manual mode.

There are class instances for the SBIG camera, the ASI-cameras, the mount and the dome. Except for the ASI-camera, indilib is used for access to this devices. The ASI-cameras are accessed via the SDK. To start the former, an indiserver has to be started and connected with the devices. This is done by the method "start()", which each of those classes has.

```
In [1]: info

Information about the MAM-Teleskop:
Dome is connected
Dome is closed
Telescope is connected
Telescope is tracking sidereal
Telescope's target is Vega
Telescope is not in park position
Telescope is pointing to Ra: 018.63, Dec: 038.80
Main camera is connected
Guide camera is connected
Slit camera is connected

Connection to Arehucas: OK
Weather is irrelevant, but OK

RCU information:
{'ThAr': False, 'Flat': False, 'Mirror': False}

Currently running: Nothing;

In [2]: □
```

Figure 22. Screen shot of the interpreter displaying the current status. (Weather irrelevant means that the interpreter is in manual mode and therefore not handling weather warnings.)

The interpreter normally doesn't execute the bare python code, even though it could. Instead, commands of a given list are executed that are implemented as a dict of functions. At start up of the software, the available commands are listed.

The class instances for the three cameras, the mount and the dome are Cam (SBIG), Spalt (slit), Guide (secondary camera), Tel (mount) and Dom (dome). In the regular commands that expect one of these, they can be written in lower case as well.

help:

If this is used without an argument, the introductory list of commands is shown. If it is used with a function or object as argument, the docstring is displayed.

info:

This takes no arguments and prints the current status of the telescope like presented in [Figure 22](#).

pCycle:

This function power cycles the device that is given as argument. 1/Cam, 2/RCU, 3/Mount, 4/USB or ASI. To power cycle the ASI-cameras, the USB hubs are power cycled combined with a reboot, so it is recommended to do this manually.

SwPower:

Similar to this, the power of the four power switches can be set via this command, while the first argument is the device and the second one is either on or off. The device can also be "*" to set the power of all devices. If no second argument is given, the status of the power control switches is printed instead.

rcu:

This command accesses the RCU. The arguments can be 0, 1, 2 and 3, while 1-3 switch on/off

the Thorium-Argon-lamp, the flat field halogen lamp and the reference mirror respectively, 0 switches all three off.

state:

With state, the current state of the RCU is printed out.

exit:

exit leaves the interpreter equivalent to ctrl+D. Unlike the latter, it accepts two parameters: indi and pow. If the argument indi is passed, the indiserver will keep running and if pow is given, the devices are not powered off afterwards.

Note that these are obsolete if another instance is running, since the other process is holding them back.

start/startall:

"start" starts the indiserver of all devices that are given as arguments.

open/close:

Self explaining, they open/close the dome shutter.

weather:

This command reads the CC-report. If the software is running in manual mode, it just prints if a weather warning is caught. Else, it reacts to the weather warnings and received target objects automatically. This includes, that the measurement starts, if the CC-report includes valid coordinates.

The command is automatically executed regularly, except in manual mode.

bin:

This sets the binning of a camera. The first argument is the camera, the second the (always quadratic) binning (1, 2 or 3).

light:

Take a normal image with the main camera. The not ordered arguments are the file path and the exposure time. If no filepath is given, the image is displayed.

flat/thar:

Like light, but it automatically toggles the rcu to the correct state.

dark:

Like light, but keeping the camera shutter closed.

bias:

Take an image with minimal exposure time and closed shutter. As argument, the number of iterations can be given. The result than will be the average of them.

focus:

Repeatedly take an image with the selected camera (first argument) with a exposure time given by the second argument and display it.

spalt:

Take an image with the slit camera. Possible parameters are the exposure time, the file path and "low". The latter one causes an 8-bit image instead of a 16-bit one and skips the median filter normally used (to avoid hot pixels to be seen as stars while tracking).

guide:

Like spalt, but for the secondary camera and without median filter.

goto:

Slew to a object in the sky. Argument can either be RA:DEC as floats (h:d), or the name of the object. The parameter "-h" prevents the automatic star to slit correction.

add:

Needs two arguments: Ra and Dec. Corrects the current position respectively.

track:

If no argument is given, the tracking is switched on/off altering. Possible arguments are "sideral", "lunar" and "solar" to select the tracking mode.

target:

All measured spectra need a reference spectrum that is used as the "ideal transmission" for analysis. To distribute the reference images to the spectra, as well as to process these, the command "target" is used. To select a target, the target number is given as argument to the command.

targetlist:

"targetlist" prints out the targets stored with their corresponding number that is needed to edit the target.

stop:

Stops the telescope. As argument, "measurement" can be given. This stops the measurement procedure started by the CC-report.

mkref/midas/upref:

See below.

pipe:

Gives the specified images to MIDAS to analyse them. To move the results and the spectral plots to a given place, the folder can be stated with "name=folder_name" as argument. All other arguments are seen as paths to images.

3.2.5 Data calibration

The calibration of the pictures is done with MIDAS via Baaders Virtual Box image MIBAS. ESO-MIDAS (European Southern Observatory - Munich Image Data Analysis System) is a powerful software tool developed by the ESO for analysis and processing of celestial image data.

To do the calibration the command "mkref" is used in the way:

```
mkref FlatExposureTime=25 ThArExposureTime=40
```

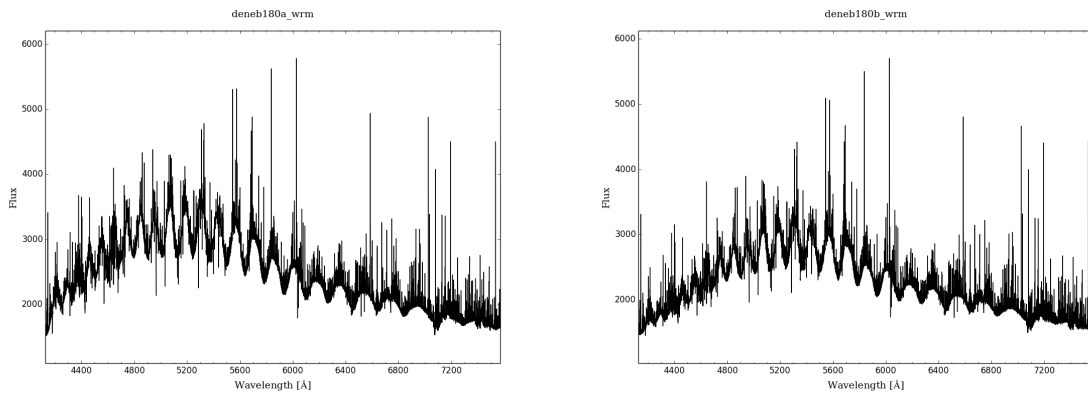


Figure 23. Spectrum of Deneb on Jan. 15. 2020 at 21:35 (a) and 21:49 (b).

while the times are given in seconds. This will take the ordref and thar-lamp images accordingly and pass them to the virtual box. Then the direct continuation with the calibration is possible if desired.

To use existing reference images instead, the command "midas" is used in the same way, while the exposure times just define the existing images that are to be used. After start up of the calibration with MIDAS either through continuation after "mkref" or directly through "midas" the interpreter directly returns and midas is X-forwarded from the virtual box in a subthread. The result of the analysis are in fits format and can be plotted. (See Figure 23 for example). To refresh the calibration instead, one has to use:

```
upref FlatExposureTime=None ThArExposureTime=None
```

If no exposure times are given the last ones used are taken.

The detailed instructions for the further process are described in the [MIBAS manual](#).

To analyse a taken spectrum, knowledge of the light spectrum of the observed star is required. For the moment, a collection of spectra of the star is used taken under very good observation conditions at a zenith angle close to 0. This, of course, is not sufficient, since "very good conditions" is not clearly defined and, more importantly, not always possible. Therefore, in the future a model could be used that describes the theoretical expected spectrum of the star based on its spectral class and brightness. This could maybe be combined with the current method.

3.2.6 Additional telescope tube and secondary camera

At first, the secondary camera should be used as a guiding camera. But it can probably be better used for photometry, since the image of the slit camera is large enough to be used for guiding as the images can be passed to astrometry. The problem is that stars are not perfectly at a point, but are moving slightly due to atmospheric turbulence. Therefore a darker spectrum cannot only be the result of lower atmospheric transmission, but also of the star not hitting the slit permanently due to turbulences. To distinguish those two cases, the crosscheck with the photometry is needed.

The full manual and the documentation is on the wikipage of MAGIC.

4 Measurement test run

To test the working of the new system the processed data of a test run is compared to the data of LIDAR and to the default atmosphere model. This was done remotely via ssh with the manual control interface of the MAM software.

4.1 Measured object

The test run was done on the night of the 28th to 29th of February 2020 using the star Regulus (α -Leonis) as target. The measurements were done at different zenith angles to obtain the development of the transmission in dependency of the air mass. The first measurement was started at 1:00 UTC with an air mass of about 1.1, the second measurement was started at 4:00 UTC with an air mass of about 1.8 and the last measurement at 6:00 UTC, with an air mass > 3 . The night started with rather good observation conditions, but at the end of the observations clouds appeared. (See also Figure 24.) Dawn was at 6:38 UTC.

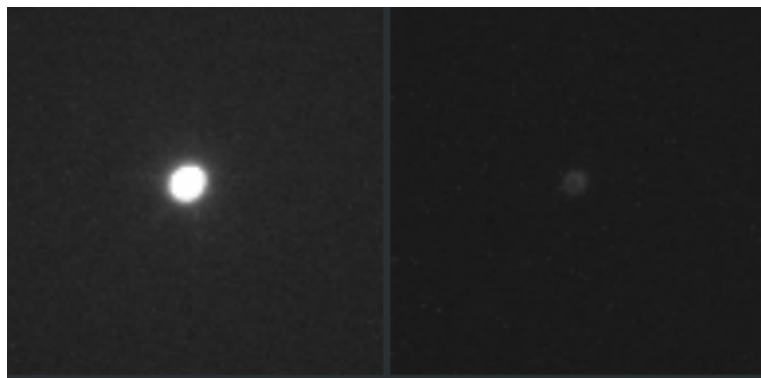


Figure 24. Regulus seen through the secondary camera at 5:53 (left) and 6:13 (right). The right image is less bright through the appearance of a aerosols in front of Regulus, probably normal clouds.

The full data taken from Regulus is shown in Appendix A.

As it can be seen, the red component of the light is decreasing not as fast as the blue with increasing zenith angle, which is caused by the scattering of the light as described in Section 2.

To determine the atmospheric transmission from the absolute intensities measured by the main camera, they have to be divided by the theoretical intensity one would obtain if no atmosphere would be present, i.e. with air mass $X=0$. Therefore, an exponential fit was done on the data of the 1 and 4 o'clock measurement. The resulting spectral intensity is shown in Figure 27. Since the fit was done over all wavelengths, not all fits can be shown here. As an example, the fit for one wavelength is shown in Figure 33 in Appendix A.

The uncertainties are marked as grey area, but since this is not visible well, they are plotted also separately in Figure 28.

Now the measured spectral intensities were divided by reconstructed original spectral intensities of the star. The results are shown in Figure 29.

The transmission of the 72° zenith angle measurement was already under the heavy influence of the upcoming clouds. Still, the signal is not zero compared to the 89.4° measurement (see figures in the Appendix A)

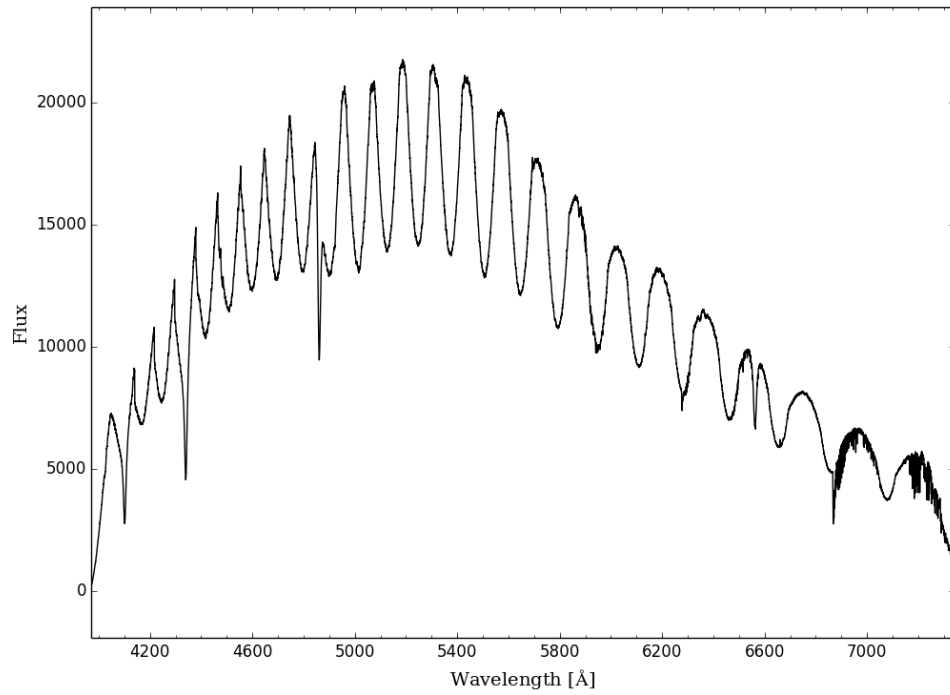


Figure 25. The spectral light intensity of Regulus at air mass = 1.05.

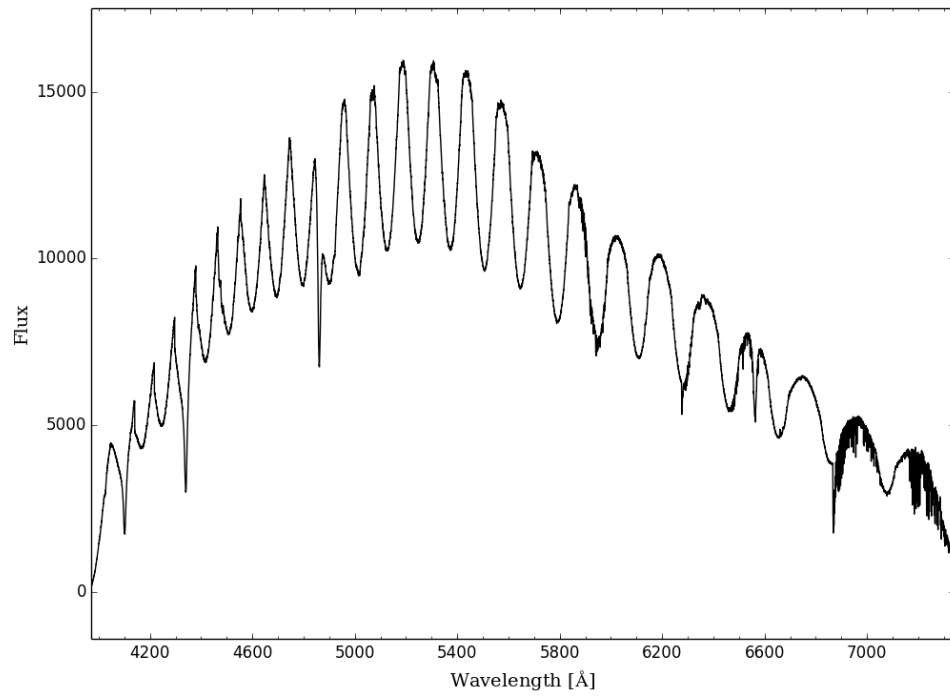


Figure 26. The spectral light intensity of Regulus at air mass = 1.77.

4. MEASUREMENT TEST RUN

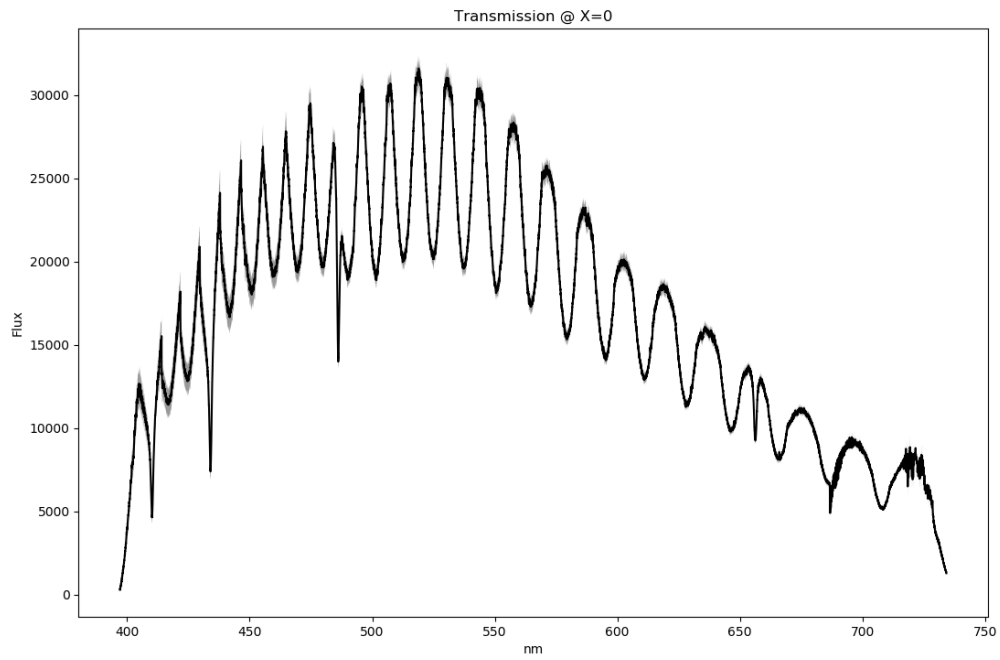


Figure 27. The spectral light intensity of Regulus estimated to be measured outside the atmosphere.

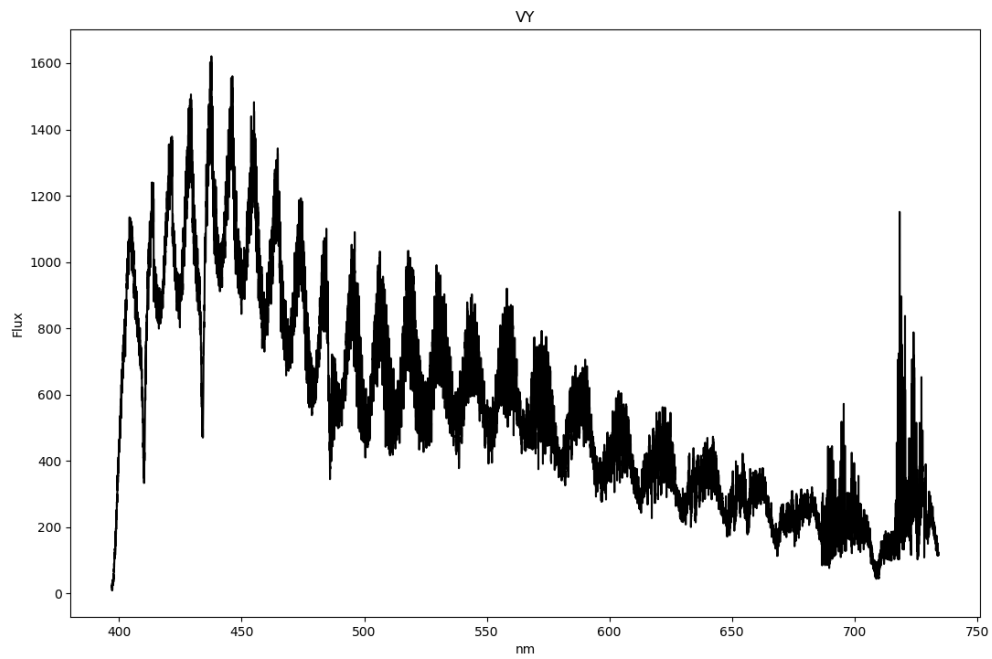


Figure 28. The uncertainty of the plot in Figure 27.

4. MEASUREMENT TEST RUN

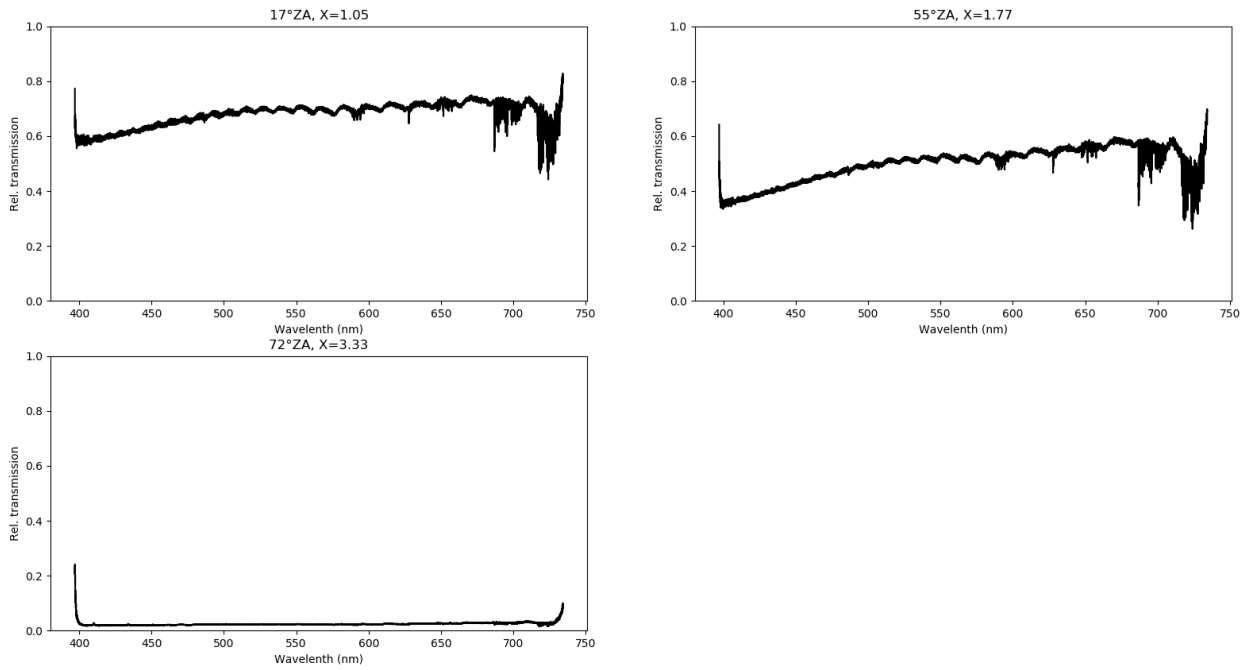


Figure 29. The measured transmission of the atmosphere at different zenith angles.

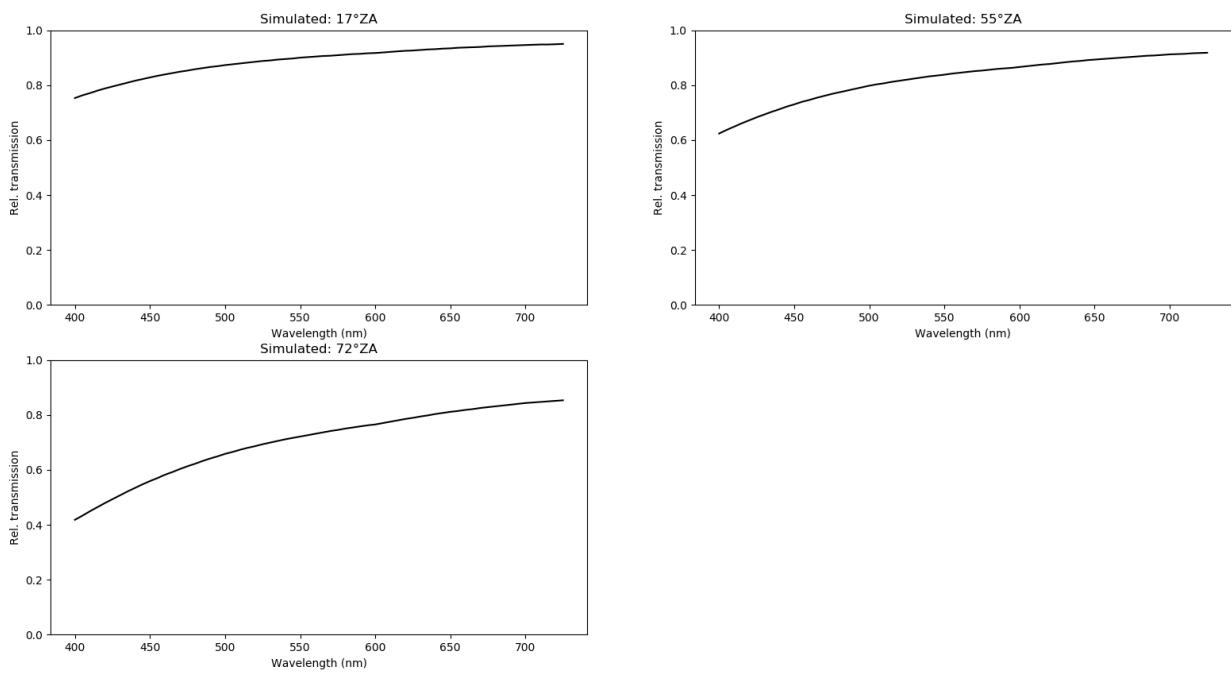


Figure 30. The theoretical transmission of the atmosphere at different zenith angles.

4.2 Comparison with the atmospheric model

The theoretical atmospheric model used by MAGIC provides the atmospheric transmission under perfect circumstances i.e. no aerosols in the air at all. The transmission calculated with the model are summarized in Figure 30.

The qualitative shape of the measurement is consistent with the theoretical model: The transmission of blue light decreases faster with increasing zenith angle than the one of the red light. The differences are small fluctuations as well as an overall lower transmission of about 20 percent. The first are expected due to not perfect aerosol free atmosphere. The latter suggests that the reference measurements at low zenith angle were not done under good enough atmospheric conditions.

Furthermore, one can see that the instrument function (wavelength dependent sensitivity of the instrument/camera) is not completely cancelled out which leads to the small wobbles in the line, but this effect is small enough to be neglected.

At the borders of the sensitive region of the spectrum (400 nm and 750 nm) the values of the data were very low, so little noise fluctuations were drastically changing the result after the division through the reference intensity. Therefore this areas do not contain valid data.

4.3 Comparison with photometry of the secondary camera

To compare the transmission with photometry, the relative transmissions were integrated over the wavelengths and then divided by the wavelengths. For photometry, the images with luminance filter where used. The luminance filter has a similar wavelength range as the analysed spectra (compare Fig. 31 and 27) and is therefore good for comparison.

The light intensity of stars in the images were determined with IRIS. Similar to the spectra, the light intensity of the images were divided by the extrapolated intensity corresponding to air mass equal to zero. This results in the "white light" transmission shown in Table 1 and in Figure 32.

Air mass	Spectra Transmission [%]	Air mass	Photometry Transmission [%]
1.049	67.99±0.16	1.065	59.4±0.8
1.055	64.88±0.16	1.069	59.2±0.8
1.073	64.76±0.16	1.073	59.3±0.8
1.592	53.31±0.13	1.592	45.6±0.6
		1.623	45.0±0.6
		1.655	43.9±0.6
1.735	50.86±0.12	1.689	44.0±0.6
1.773	49.64±0.12	1.773	42.7±0.6
3.334	2.290±0.006	3.334	11.5±0.2
4.413	1.265±0.003	4.413	5.39±0.07
4.805	0.444±0.001	4.805	1.50±0.02
5.722	0.357±0.001		

Table 1. Integrated transmission obtained by the spectra (left) and by photometry (right).

As one can see in Figure 32, the photometric data is closer to the theoretically expected exponential decay. This suggests, that there is a measuring error in the spectral measurements: Due to seeing (small movements of the star due to thermal fluctuations in the atmosphere) and due to vibrations of the telescope, the star is not hitting the slit of the spectrograph for

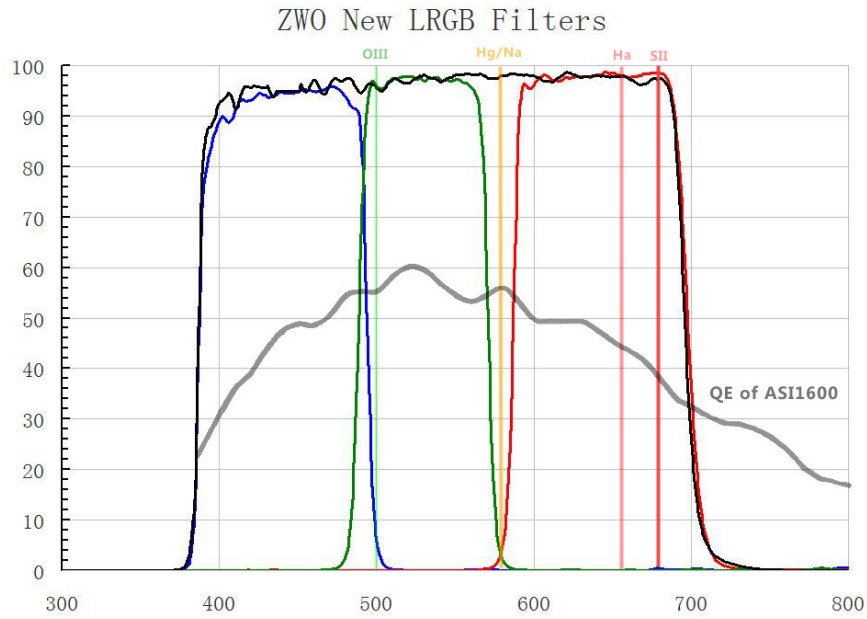


Figure 31. Wavelength dependent transmission of the filters (red, green, blue, black for the r, g, b and luminance filter) in the secondary camera. QE is the quantum efficiency of the CMOS sensor.[20]

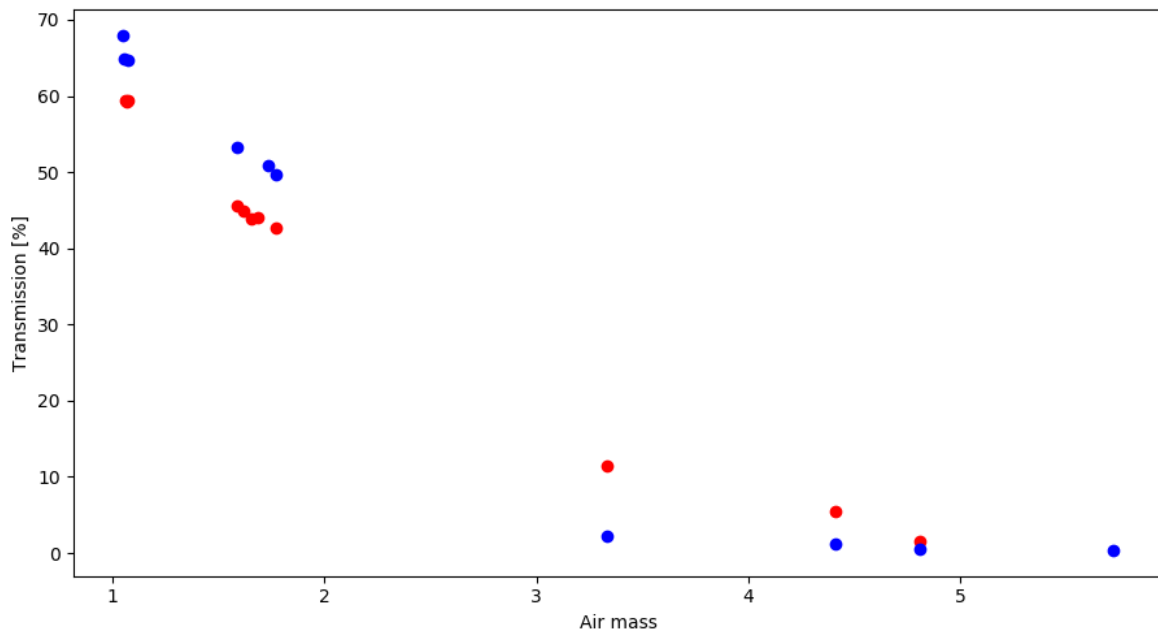


Figure 32. Integrated transmission obtained by the spectra (blue) and by photometry (red).

the full exposure. Since this increases with the air mass, the signal gets weaker with increasing air mass. This will be corrected in the future by using the photometric data to adjust the total intensity of the spectra, since photometry is not influenced by the seeing or vibrations. It is necessary to use the information of the rgb filters as well, since aerosol scattering can lead

to a halo around the star that would make the photometric data incorrect. But by comparing the different colour images this can be distinguished from seeing. Seeing is approximately equivalent for all wavelengths, the scattering not.

4.4 Comparison with the LIDAR results

LIDAR measured a distance dependent transmission as presented in Table 2.

Reference distance	3 km	6 km	9 km	12 km
Transmission [%]	42.1556	41.8776	38.2202	38.1916

Table 2. Transmission around Regulus measured by LIDAR during the 6 o'clock measurement.

Assuming the height of the atmosphere is 12 km (outside the troposphere the extinction is very small) an extrapolation was done. This means that air mass = 1 corresponds to 12 km of atmosphere thickness. The resulting extrapolation is shown in table 3

Air mass:	3.334	4.413	4.805	5.722
Transmission [%]	26±3	22±4	20±4	18±4

Table 3. Transmission extrapolated from LIDAR data.

Comparing these values to the ones measured with MAM (see Table 1) one can see that the extrapolated values are too high. This is caused by aerosols/clouds absorbing the light further than 12 km away from the telescopes, since LIDAR can't measure that far.

On the other hand, LIDAR measured a transmission of 87.11 % at a zenith angle of 19.07° with good observation conditions (27th of February). Since LIDAR and the simulation are differing from the measurements of MAM here, it can be assumed that the reference measurements of Regulus at low zenith angle were not perfect. Therefore further reference measurements should be done when the atmospheric conditions are better.

5 Conclusion and outlook

MAM, the new subsystem to MAGIC, will provide valuable additional data that is needed for VLZA observations. The existing data are not sufficient, since LIDAR has limited range and is therefore not as useful at VLZA. The theoretical model on the other hand has no information on the current atmosphere status. Since especially at VLZA there is a high risk of absorbing aerosols in the air and their appearance can change quickly, the theoretical model is not useful here. MAM solves these problems. It measures the current atmospheric transmission at the observed region in the sky. Furthermore, it has two separate ways of measuring the transmission that allow crosschecking the measured data. Additionally, it gives the full wavelength dependent transmission and not just that of one single wavelength like LIDAR does.

As the evaluation of the data of the first test measurement has shown, the telescope and the software do work in principle. Now there is need for a big set of good quality reference data to be able to process the measured spectra and the photometric images correctly.

Since not every star can be observed under good atmospheric conditions at low zenith angle, it can be useful for the future to generate models that describe the reference data in dependence of the magnitude and the spectral class or known spectra of the observed star. The reference data generated by the model would give the data one would obtain when measuring the corresponding star with the MAM instruments outside of the atmosphere.

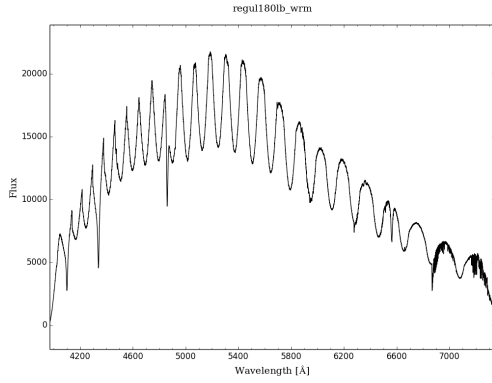
It is also necessary to correct for the seeing effect, i.e. the effect that the star projection is randomly moving around the slit. For this, the data of the photometry will be used. Possibly the images of the slit taken during holding the star on the slit by the software can be used for this as well.

Another possible improvement would be that the star selection is not restricted to one star. Instead, dependent on the amount of available stars and the observation duration of the current target, a bunch of reference stars can be selected, between which the telescope cycles through.

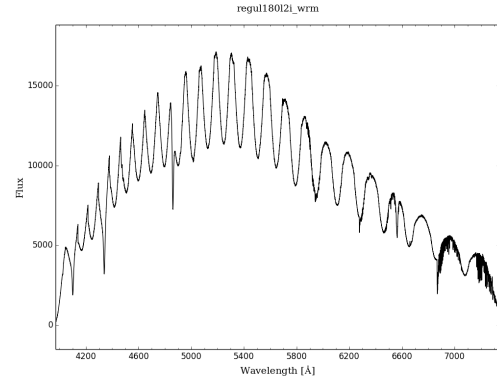
Appendix

A Data

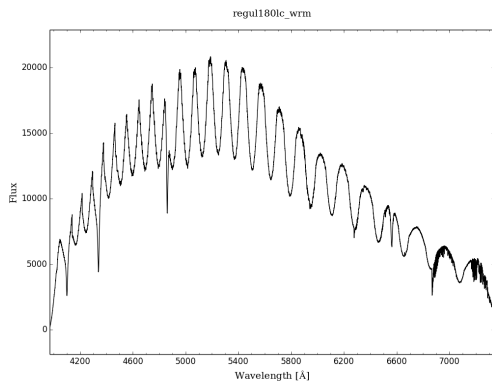
Regulus 29.2.20



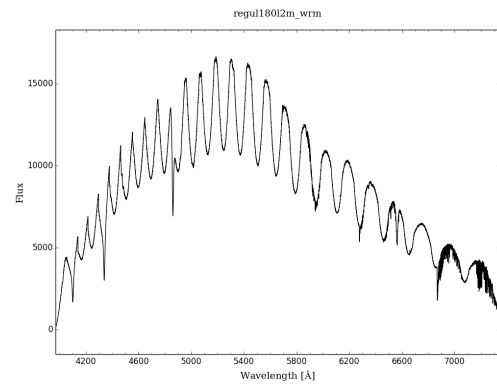
The light intensity of Regulus at air mass = 1.049.



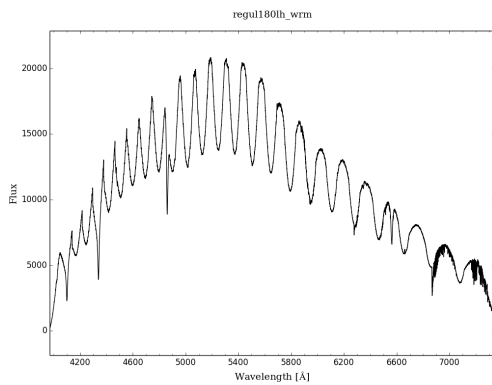
The light intensity of Regulus at air mass = 1.592.



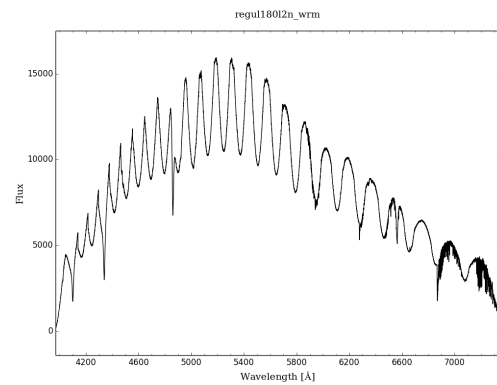
The light intensity of Regulus at air mass = 1.055.



The light intensity of Regulus at air mass = 1.735.

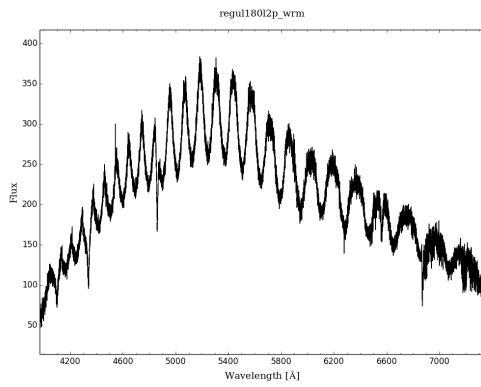


The light intensity of Regulus at air mass = 1.073.

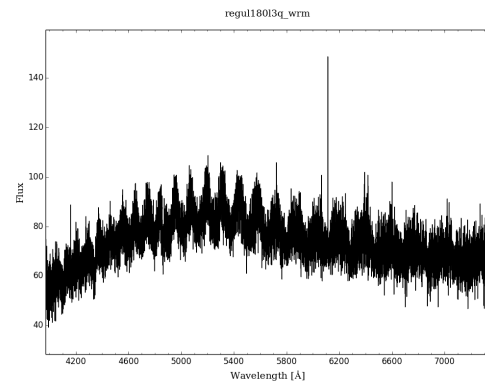


The light intensity of Regulus at air mass = 1.773.

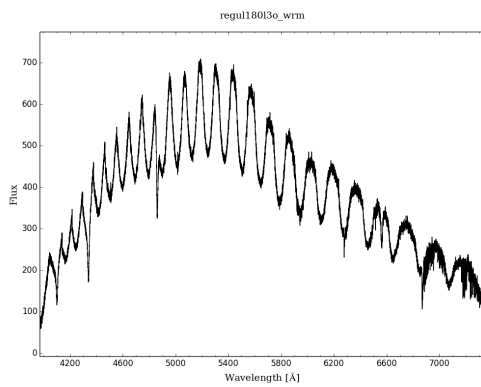
A. DATA



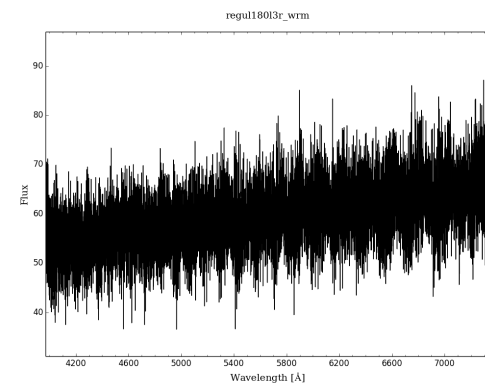
The light intensity of Regulus at air mass =
4.413.



The light intensity of Regulus at air mass =
4.805.



The light intensity of Regulus at air mass =
3.334.



The light intensity of Regulus at air mass =
5.722.

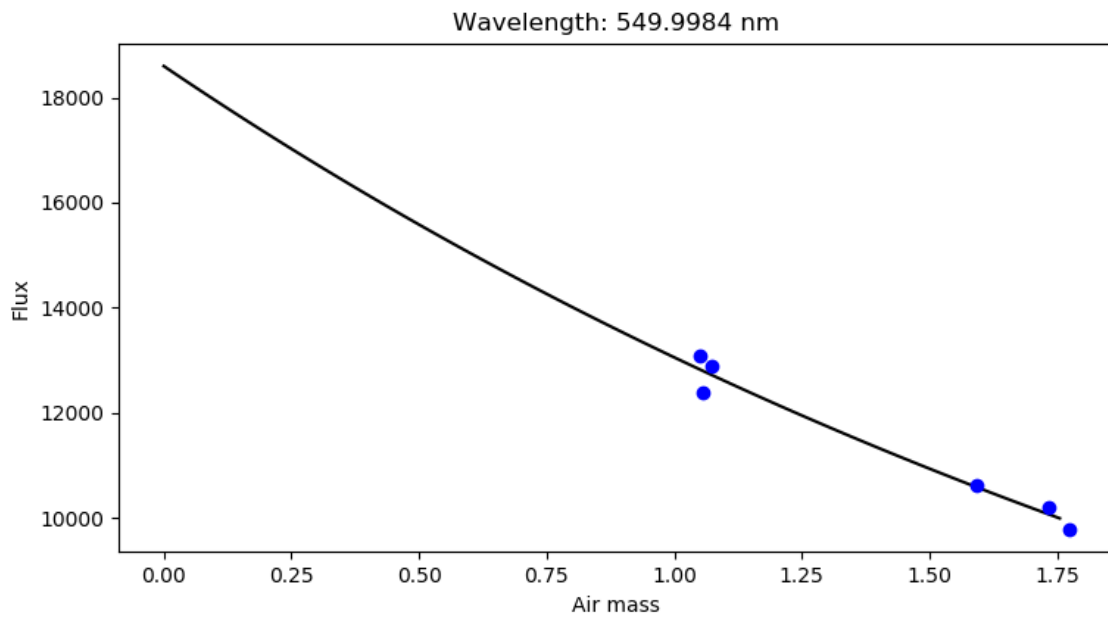


Figure 33. Exemplary extrapolation to air mass = 0 with $I = I_0 e^{a \cdot X} \approx 18595 \cdot e^{-0.353 \cdot X}$.

B Source code

The source code of the control software can be found on:

https://www.mpp.mpg.de/~dhoff/MAM_Control/

References

- [1] Official MAGIC website:
<https://magic.mpp.mpg.de/>
Accessed 2020-02-04
- [2] A. M. Hillas et al. The spectrum of tev gamma rays from the crab nebula. *The Astrophysical Journal*, 503(2):744, 1998.
<http://stacks.iop.org/0004-637X/503/i=2/a=744>.
- [3] HESS:
https://en.wikipedia.org/wiki/High_Energy_Stereoscopic_System
Accessed 2020-02-04
- [4] VERITAS:
<https://en.wikipedia.org/wiki/VERITAS>
Accessed 2020-02-04
- [5] Cosmic rays:
<https://masterclass.icecube.wisc.edu/sites/default/files/images/cr-energy-icetop.png>
Accessed 2020-01-20
- [6] Crab nebula:
https://en.wikipedia.org/wiki/Crab_Nebula#/media/File:Crab_Nebula.jpg
Accessed 2020-02-04
- [7] C. Fruck: *A new LIDAR system for the MAGIC telescopes and site search instrumentation for CTA*, Munich, 2011
- [8] MAGIC site:
https://magicold.mpp.mpg.de/gallery/pictures/IMG_0623.JPG
- [9] Cherenkov radiation:
<https://de.wikipedia.org/wiki/Tscherenkow-Strahlung>
Accessed 2020-02-04
- [10] Analysis methods for Atmospheric Cerenkov Telescopes:
https://www.mpi-hd.mpg.de/hfm/HESS/pages/publications/proceedings/Conf_Palaiseau_2005/deNaurois.pdf
Accessed 2020-03-12
- [11] Konrad Bernlöhr. Impact of atmospheric parameters on the atmospheric cherenkov technique. *Astroparticle Physics*, 12(4):255 – 268, 2000.
<http://arxiv.org/abs/astro-ph/9908093>
- [12] Calima:
<https://de.wikipedia.org/wiki/Calima>
Accessed 2020-02-04
- [13] Rayleigh scattering:
https://en.wikipedia.org/wiki/Rayleigh_scattering
<https://de.wikipedia.org/wiki/Rayleigh-Streuung>
Accessed 2020-02-04

- [14] Mie scattering:
https://en.wikipedia.org/wiki/Mie_scattering
Accessed 2020-02-04
- [15] Mie scattering:
<http://hyperphysics.phy-astr.gsu.edu/hbase/atmos/blusky.html#c1>
Accessed 2020-02-04
- [16] Baches Echelle Spektrograf manual:
https://www.baader-planetarium.com/de/downloads/dl/file/id/312/product/0/baches_echelle_spektrograf_tutorial_76_seiten.pdf
- [17] CCD:
<https://de.wikipedia.org/wiki/CCD-Sensor>
Accessed 2020-02-10
- [18] Airy disk:
https://en.wikipedia.org/wiki/Airy_disk
Accessed 2020-03-18
- [19] Lambert-Beer-law:
https://de.wikipedia.org/wiki/Lambert-Beer'sches_Gesetz
Accessed 2020-03-18
- [20] ZWO ASI Filter:
<https://astronomy-imaging-camera.com/wp-content/uploads/RGBL-ASI1600.jpg>
Accessed 2020-03-19